Available online at www.sciencedirect.com
ScienceDirect
Acta Materialia 59 (2011) 4229–4234
Acta MATERIALIA
www.elsevier.com/locate/actamat

First-principles lattice dynamics and heat capacity of $BiFeO_3$

Yi Wang *, James E. Saal, Pingping Wu, Jianjun Wang, Shunli Shang, Zi-Kui Liu, Long-Qing Chen

Materials Science and Engineering, The Pennsylvania State University, University Park, PA 16802, USA

Received 15 November 2010; received in revised form 13 February 2011; accepted 17 March 2011
Available online 12 April 2011

Abstract

We study the lattice dynamics of bismuth ferrite ($BiFeO_3$) rhombohedral ferroelectric ($R3c$) using first-principles density functional theory calculations and the direct force constant method. We determine the phonon dispersions, phonon density of states, and heat capacity. Special attention is paid to the heat capacity at low temperature, at which the present phonon calculations show significant deviations from the Debye-like T^3 behavior until $T \leqslant 7$ K. Based on the excellent agreement between the measured and calculated curve shapes of the heat capacity we propose that no gapped magnon modes exist for $BiFeO_3$ that contribute to the heat capacity of $BiFeO_3$ in the temperature range 5–30 K.

Keywords: $BiFeO_3$; First-principles phonon theory; Heat capacity; Phonon dispersion

1. Introduction

Bismuth ferrite ($BiFeO_3$) is being extensively studied [1–4] as a room temperature multiferroic material [5]. It possesses high spontaneous electric polarization below the ferroelectric Curie temperature (T_C) of 1120 K and exhibits antiferromagnetic order below the Néel temperature (T_N) of 640 K.

Numerous experimental and theoretical works on $BiFeO_3$ have been published in the literature in terms of zone center phonon modes [6–11], polarization [12–14], heat capacity [2,15–17], and magnetic phase transition [18–23]. However, as pointed out by Lu et al. [2], many experiments suffer from effects such as impurity phases, magnetic defects, or deviations from the ideal oxygen stoichiometry, resulting in the observation of weak ferromagnetism and a number of further magnetic or structural phase transitions at low temperatures.

In general, an accurate determination of the heat capacity as a function of temperature could help resolve the problem of whether a magnetic phase transition has occurred. As a fundamental property of a solid the heat capacity can provide the characteristic fingerprint of the electronic, magnetic, and superconductive properties and phase transitions. This is especially true at low temperatures. For instance, the contributions to the heat capacity of electron, magnon, and lattice vibrations are proportional to T, $T^{1.5}$, and T^3, respectively [24]. Recently, detailed investigations of the heat capacity of high-quality single crystals of $R3c$ $BiFeO_3$ have been reported from 2 K up to room temperature by Lu et al. [2]. They found that no experimental evidence was seen for spin glass ordering, and the absence of anomalies in the temperature dependence of heat capacity signals a lack of any structural or magnetic phase transitions below room temperature. Using the Debye T^3 law to analyze the low-temperature heat capacity data, Lu et al. [2] proposed the existence of an anisotropy gap of the magnon modes of the order of 6 meV.

However, it should be noted that many ferroelectric materials [25–33] do not obey the predictions of the Debye model until very low temperatures, which may reflect the fact that the phonon density of states (DOS) (i.e. the vibration spectra) of real materials are more complex than the

* Corresponding author.
E-mail address: yuw3@psu.edu (Y. Wang).

1359-6454/$36.00 © 2011 Acta Materialia Inc. Published by Elsevier Ltd. All rights reserved.
doi:10.1016/j.actamat.2011.03.047

Debye model assumption that ω^2 (the square of the phonon frequency) is proportional to the phonon DOS. Accordingly, an accurate first-principles thermodynamic calculation based on the phonon theory for the $R3c$ phase of $BiFeO_3$ presents a unique opportunity for a proper understanding of $BiFeO_3$. However, the existing phonon calculations [6,10,34–38] are either not for the ground state $R3c$ phase of $BiFeO_3$ or just for the Γ point and, hence, did not calculate the phonon dispersions and heat capacities for the $R3c$ phase.

In this work we report first-principles calculations of phonons and the heat capacity for the ground state antiferromagnetic $R3c$ phase of $BiFeO_3$. The focus is on the heat capacity at low temperatures. Our theoretical results indicate that the interpretation of the measured thermal data for high-purity samples [2] as being a result of "a magnon gap" or "extra modes" is questionable.

The challenge in calculating the phonons of $BiFeO_3$ is the fact that $BiFeO_3$ is a Mott–Hubbard insulator [16], involving a polar effect of and strong correlation among the d electrons of Fe. The polar effect [39] results in splitting between the longitudinal optical (LO) and transverse optical (TO) phonon modes. In this work we treat the polar effect using a mixed space approach [40,41] and the strong correlation using the Dudarev DFT+U method [42].

2. Direct approach to phonons of polar materials

The present work adopts the direct method to obtain the phonon frequencies, i.e. the inter-atomic force constants are directly calculated in real space using a supercell. Since $R3c$ $BiFeO_3$ is a polar material, it is important to properly treat the contribution of the non-analytical term which results in LO–TO splitting. Recently we have shown that using a mixed space approach it is possible to accurately determine [40,41] the phonon frequencies of polar materials without fitting parameters. The mixed space approach solved the long-standing problem within the direct approach in calculating the contribution of long-range dipole–dipole interactions. The real space force constant, $\Phi^{jk}_{\alpha\beta}$, between atom j in the primitive cell M and atom k in the primitive cell P can be expressed as

$$\Phi^{jk}_{\alpha\beta}(M,P) = \phi^{jk}_{\alpha\beta}(M,P) + \frac{1}{N}\tilde{D}^{jk}_{\alpha\beta}(na;\mathbf{q} \to 0) \tag{1}$$

where $\phi^{jk}_{\alpha\beta}$ is the contribution from short-range interactions, N the number of primitive unit cells in the supercell, and $\tilde{D}^{jk}_{\alpha\beta}(na;\mathbf{q} \to 0)$ is the contribution from long-range interactions, i.e. the so-called non-analytical part of the dynamical matrix in the limit of zero wave vector $\mathbf{q}$. According to Cochran and Cowley [39]

$$\tilde{D}^{jk}_{\alpha\beta}(na;\mathbf{q} \to 0) = \frac{4\pi e^2}{V}\left.\frac{[\mathbf{q}\cdot\mathbf{Z}^*(j)]_\alpha[\mathbf{q}\cdot\mathbf{Z}^*(k)]_\beta}{\mathbf{q}\cdot\boldsymbol{\varepsilon}_\infty\cdot\mathbf{q}}\right|_{\mathbf{q}\to 0} \tag{2}$$

where V is the volume of the primitive unit cell, $\mathbf{q}$ is the wave vector, α and β are the Cartesian axes, $\mathbf{Z}^*(j)$ is the Born effective charge tensor of the jth atom in the primitive unit cell, and $\boldsymbol{\varepsilon}_\infty$ is the high-frequency static dielectric tensor, i.e. the contribution to the dielectric permittivity tensor from the electronic polarization [43]. Therefore, the dynamical matrix $\tilde{D}^{jk}_{\alpha\beta}(\mathbf{q})$ can be straightforwardly calculated by the Fourier transformation [44]:

$$\tilde{D}^{jk}_{\alpha\beta}(\mathbf{q}) = \frac{1}{\sqrt{\mu_j\mu_k}}\frac{1}{N}\sum_{M,P}\Phi^{jk}_{\alpha\beta}(M,P)\exp\{i\mathbf{q}\cdot[\mathbf{R}(P)-\mathbf{R}(M)] \tag{3}$$

where μ_j is the atomic mass of the jth atom in the primitive unit cell and $\mathbf{R}(P)$ is the position of the Pth primitive unit cell in the supercell.

3. Computational details

The primitive unit cell of $R3c$ $BiFeO_3$ contains 10 atoms [2]. We treat the spins of the two Fe atoms as anti-parallel in the primitive unit cell so that it preserves the antiferromagnetic order with G-type spin configuration. For first-principles static calculations at 0 K, we employ the projector-augmented wave (PAW) method [45,46] together with the Dudarev DFT+U method [42] implemented in the Vienna ab initio simulation package (VASP, version 5.2). The calculated results using the Dudarev DFT+U approach only depend on the difference U–J. The proper choice of the value of U–J is dependent on the properties to be calculated. Neaton et al. [12] tested U–$J = 0$, 2, and 4 eV in their local spin density approximation (LSDA) plus U calculation and found U–$J = 2$ is good for the electronic and magnetic properties. In comparison, Kornev et al. [47] found U–$J = 3.8$ eV is best in developing their effective Hamiltonian scheme to study the finite temperature properties of $BiFeO_3$ within LSDA+U. By experience, large values for U–J are preferable when calculating phonon properties of strongly correlated systems. [16,41,48–50] Therefore, we use U–$J = 6.0$ eV for the d orbital of Fe. The exchange correlation functional of the generalized gradient approximation (GGA) [51] is employed in all calculations. Although the calculated local magnetic moment for the Fe atom is 4.26 μ_B. which is somewhat larger than the experimental value of 3.75 μ_B from Sosnowska et al. [52], the calculated band gap with U–$J = 6.0$ eV is 2.46 eV which is in good agreement with the experimental value of 2.5 eV measured by Gao et al. [53] and 2.75 eV measured by Ihlefeld et al. [54]. In comparison, the calculated local magnetic moment for the Fe atom is 3.8 μ_B and the calculated band gap is 1.3 eV in Neaton et al. [12] with U–$J = 2$ eV within LSDA+U. To calculate the Born effective charge tensor we employ the linear response approach implemented in VASP 5.2 by Gajdos et al. [55] The 0 K static calculations are conducted at five volumes near the equilibrium. At each volume both cell shape and internal atomic positions are optimized with a Γ-centered $11 \times 11 \times 11$ k mesh, an energy cut-off of 500 eV, and a total energy convergence threshold of 10^{-8} eV. In calculating the real space force constants we

use the linear response approach together with 80 atom $2 \times 2 \times 2$ supercells, a Γ-centered $5 \times 5 \times 5$ k mesh, and an energy cut-off of 400 eV. To obtain smooth phonon DOS sampling of the **q** space is made using a $100 \times 100 \times 100$ mesh, which results in 30,000,000 phonon frequencies.

4. Results and discussion

The calculated structural parameters of $R3c$ $BiFeO_3$ are collected in Table 1, together with the experimental data [13] and results of previous calculations [12,56]. They are expressed using the rhombohedral cell, including the Wyckoff positions, the length of the rhombohedral axis, rhombohedral angle, and the unit cell volume.

The Born effective charge tensors for the individual atoms and the high-frequency static dielectric tensor of $R3c$ $BiFeO_3$ are shown in Table 2. These data are the inputs to Eq. (2) to determine the non-analytical term to the phonon frequencies. Our calculated Born effective charges are 10–20% larger than those of Neaton et al. [12] because we have used a larger U–J value (6.0 vs. 2.0 eV). It should be mentioned that different U–J values have often been used by different authors [10,50,57]. Nevertheless, the effect of the choice of U–J on the heat capacity is not significant.

4.1. Phonon spectra

In Fig. 1 we show the calculated phonon dispersions along the direction of A–Γ–R–D–Γ for $R3c$ $BiFeO_3$ at 0 K. For a polar material the longitudinal optical phonon frequencies are dependent on the directions of approach to the Γ point, as seen from Fig. 1 from the intersection of the A–Γ and Γ–R dispersions. This behavior can be derived from Eq. (2) (for more details see Cochran and Cowley [39]). For experimental data only Γ point data are available. In Fig. 1 we have chosen to compare our calculated phonon frequencies at Γ point with the experimental infrared longitudinal and transverse optical phonon frequencies measured at 20 K by Kamba et al. [58] (as cited by Hermet et al. [35]). In the vicinity of the Γ point slightly imaginary phonon modes, i.e. unstable phonon modes with phonon frequencies smaller than 0, are found along one of the acoustic dispersions due to numerical errors. Increasing the supercell size could solve the problem. However,

Table 1
Calculated and measured structural parameters of $R3c$ $BiFeO_3$.

Atom	Coordinate	GGA+U[a]	LSDA+U[b]	GGA[c]	Experimental[d]
Bi	x	0	0	0	0
Fe	x	0.221	0.227	0.223	0.221
O	x	0.535	0.542	0.534	0.538
	y	0.940	0.943	0.936	0.933
	z	0.394	0.397	0.387	0.395
a_{rh} (Å)		5.667	5.52	5.697	5.634
α (°)		59.17	59.84	59.24	59.35
Ω (Å^3)		126.3	118.3	128.5	124.6

The Wyckoff positions are Bi(x, x, x), Fe(x, x, x), and O(x, y, z) using the rhombohedral system. a_{rh}, α, and Ω represent the length of the rhombohedral axis, the rhombohedral angle, and the unit cell volume, respectively.
[a] Results of the present GGA+U calculation.
[b] Results of the local spin density approximation (LSDA) plus U calculation of Neaton et al. [12].
[c] Results of the GGA calculation of Ravindran et al. [56].
[d] Room temperature values of Kubel and Schmid [13].

Table 2
Calculated Born effective charge tensors for the Wyckoff positions of Bi(x, x, x), Fe(x, x, x), and O(x, y, z) and the high-frequency static dielectric tensor ($\boldsymbol{\varepsilon}_\infty$) of $R3c$ $BiFeO_3$.

	xx	yy	zz	xy	xz	yx	yz	zx	zy
Bi(0, 0, 0)	4.913	4.913	4.349	−0.264	0	0.264	0	0	0
Bi(0.5, 0.5, 0.5)	4.913	4.913	4.349	0.264	0	−0.264	0	0	0
Fe(0.721, 0.721, 0.721)	3.897	3.897	3.573	0.070	0	−0.070	0	0	0
Fe(0.221, 0.221, 0.221)	3.897	3.897	3.573	−0.070	0	0.070	0	0	0
O(0.940, 0.394, 0.535)	−2.633	−3.241	−2.641	−0.252	0.618	−0.041	−0.168	0.667	−0.288
O(0.535, 0.940, 0.394)	−3.216	−2.658	−2.641	−0.296	−0.163	−0.085	0.619	−0.084	0.722
O(0.394, 0.535, 0.940)	−2.963	−2.911	−2.641	0.231	−0.454	0.442	−0.452	−0.583	−0.434
O(0.894, 0.4400.035)	−2.963	−2.911	−2.641	−0.231	0.455	−0.442	−0.452	0.583	−0.434
O(0.440, 0.035, 0.894)	−2.633	−3.241	−2.641	0.253	−0.618	0.041	−0.168	−0.667	−0.288
O(0.035, 0.894, 0.440)	−3.216	−2.658	−2.641	0.296	0.164	0.085	0.619	0.084	0.722
$\boldsymbol{\varepsilon}_\infty$	7.540	7.540	6.892	0	0	0	0	0	0

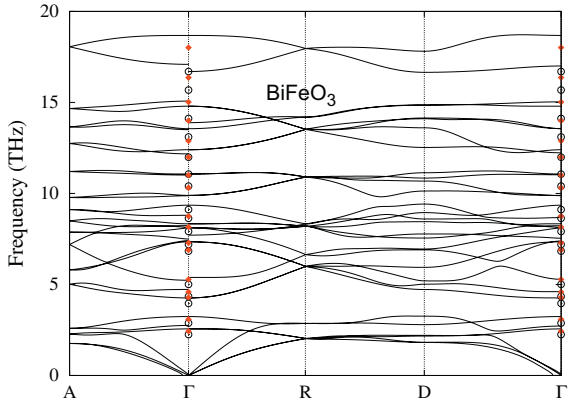

Fig. 1. Phonon dispersions of $BiFeO_3$. The solid lines represent the present calculations, the open circles and solid diamonds (red) are the experimental IR longitudinal and transverse optical phonon frequencies, respectively, measured at 20 K by Kamba et al. [58] (as cited in Hermet et al. [35]). (For interpretation of the references to color in this figure legend, the reader is referred to the web version of this article.)

increasing the supercell size will result in unaffordable computing resource costs. Nevertheless, the effects of these slightly imaginary phonon modes on the calculated phonon DOS are found to be negligible. This is demonstrated by the plot of phonon DOS in Fig. 2a, showing that the imaginary phonon modes (the region in which the frequency is smaller than 0) are barely visible in the scale of Fig. 2a.

In Fig. 2a we also plot the calculated partial phonon DOS of Bi, Fe, and O atoms, together with the total phonon DOS at 0 K using the theoretically obtained static equilibrium geometry. The major findings are that: (i) three gaps are seen in the phonon DOS around the frequencies 3.7, 11.6, and 15.9 THz; (ii) below 4 THz the phonon DOS almost completely originates from vibrations of the bismuth atoms, implying that the low-temperature thermodynamic properties of $BiFeO_3$ are dominated by bismuth; (iii) in the range 4–10 THz the phonon DOS are mainly from mixed vibrations of the iron and oxygen atoms; (iv) above 10 THz the phonon DOS is almost entirely from vibrations of the oxygen atoms.

It is known [59] that in most inelastic neutron measurements the directly measured feature is the neutron cross-section weighted phonon DOS. For the purposes of prediction and comparison with future experiments in Fig. 2b we plot the calculated generalized phonon DOS [59], i.e. where σ_i, M_i, and $pDOS_i$ represent the atomic scattering cross-section [60], the atomic mass, and the partial phonon DOS with $i =$ Bi, Fe, or O, respectively. While the phonon DOS in the low-frequency region are dominated by Bi, $\sigma_{Bi}/M_{Bi} = 0.044$ is much smaller than the values of 0.208 for Fe and 0.265 for O. Therefore, the generalized DOS in the low-frequency region is greatly reduced compared with the phonon DOS.

4.2. Heat capacity

Fig. 3 plots the calculated heat capacity together with the available experimental data [2,4,15,17]. Our results

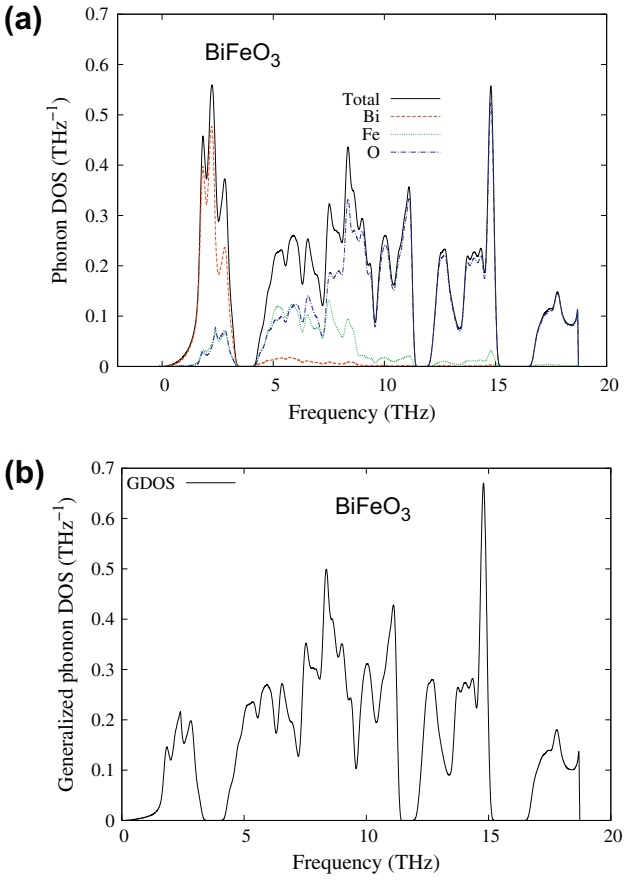

Fig. 2. (a) The calculated phonon DOS of $BiFeO_3$ where the solid, dashed (red), dotted (green), and dot-dashed curves (blue) represent the total phonon DOS and the partial phonon DOS due to Bi, Fe, and O, respectively. (b) The calculated generalized phonon DOS of $BiFeO_3$. (For interpretation of the references to color in this figure legend, the reader is referred to the web version of this article.)

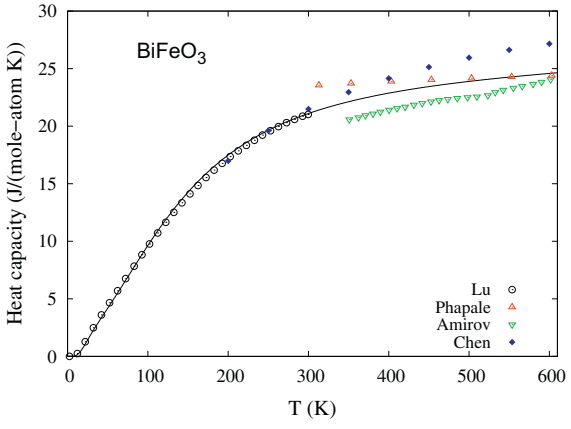

Fig. 3. Heat capacities of $BiFeO_3$. The solid line is the calculated isobaric heat capacity (C). The open circles, open triangles (red), open nablas (green), and solid diamonds (blue), represents the measured data from Lu et al. [2], Phapale et al. [15], Amirove et al. [4], and Chen et al. [17], respectively. (For interpretation of the references to color in this figure legend, the reader is referred to the web version of this article.)

agree well with the measured data of Lu et al. [2]. In analyzing the thermal properties of dielectric materials [25–33] it is useful to plot the heat capacity data as C/T^3 (C is the heat capacity) vs. temperature [61]. According to the Debye T^3 law [24] the lattice vibration contribution to C/T^3 should approach a constant at low temperatures, and hence C/T^3 vs. T plots can be employed to determine whether there are other contributions (magnetic, electronic, etc.) to the heat capacity. However, an important question is what can be considered "low temperature" in the Debye T^3 law. For example, the lattice contributions to the heat capacity due to optical phonons can easily be misinterpreted as due to other contributions [61]. It is known that the contributions due to optical phonons do not obey the Debye T^3 law.

Lu et al. made very detailed analyses of their measured data in the low-temperature region based on C/T^3 vs. T plots. They found that a pure T^3 phonon term does not provide a satisfactory fit to their low-temperature heat capacity, and they attributed the deviation from the C/T^3 law to gapped magnon modes. However, our first-principles phonon calculations seem to suggest a different reason

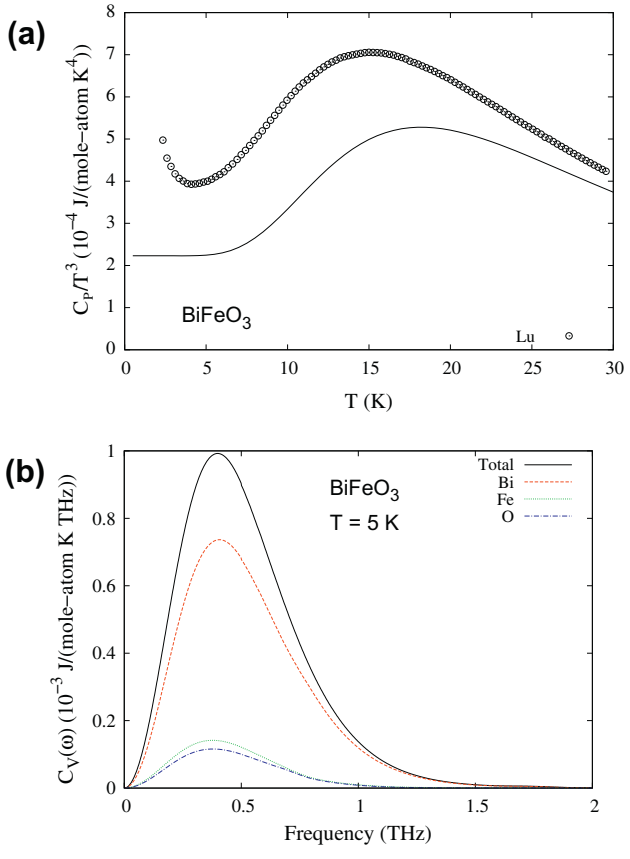

Fig. 4. (a) The calculated ($C_V(\omega)$, solid line) C/T^3 together with the measured C/T^3 from Lu et al. [2] (open circles) for $BiFeO_3$. (b) The specific contributions to the heat capacity at 5 K. The solid, dashed (red), dotted (green), and dot-dashed curves (blue) represent the total contribution and the partial contributions due to Bi, Fe, and O, respectively. (For interpretation of the references to color in this figure legend, the reader is referred to the web version of this article.)

for the deviation of C/T^3. We compare our calculated C/T^3 data with the measured values of Lu et al. in Fig. 4a. The calculated and experimentally measured C/T^3 data have maxima at ~18 K and ~15 K, respectively. Such maxima often occur in measured heat capacity measurements [25–33]. Indeed, we find that the shape of our calculated C/T^3 curve follows the measured C/T^3 of Lu et al. rather well. Consequently, we conclude that the C/T^3 deviation is due to the fact that the pure phonon contribution to the heat capacity for $BiFeO_3$ does not follow the Debye T^3 law above 7 K. Such deviations from the Debye T^3 law have been observed for many ferroelectric materials [25–33], as was pointed out by Burns [25] in 1980. We therefore suggest that no gapped magnon modes exist that can affect the heat capacity of $BiFeO_3$ in the temperature range 5–30 K. As for the numerical difference between our calculation and the measurements by Lu et al., we tentatively attribute it to traces of gapless magnons of an isotropic antiferromagnet.

In Fig. 4b we make a more detailed analysis of the specific contributions to the heat capacity at $T = 5$ K as a function of phonon frequency by atom type. We find that bismuth exclusively dominates the low-temperature lattice heat capacity. Furthermore, the contributions to the heat capacity are dictated by the phonon modes in the ~0–1 THz frequency region at 5 K.

5. Conclusions

In summary, we have presented first-principles phonon calculations for $BiFeO_3$ ($R3c$), including the phonon DOS, generalized phonon DOS, and heat capacity. We find that a pure phonon model can describe the curve shape of the heat capacity at low temperature. We show that it is not necessary to introduce an exponential term, mimicking the contribution of an anisotropy gap of the magnon excitations, in describing the temperature dependence of heat capacity for $BiFeO_3$ at low temperatures. We propose that no gapped magnon modes exist for $BiFeO_3$ that contribute to the heat capacity of $BiFeO_3$ in the temperature range 2–30 K.

Acknowledgements

This work was funded by DOE Basic Sciences under Grant No. DOE DE-FG02-07ER46417 (Y.W. and L.-Q.C.), the Office of Naval Research (ONR) under contract No. N0014-07-1-0638, and the National Science Foundation (NSF) through Grant No. DMR-1006557, and in part supported by instrumentation funded by the National Science Foundation through Grant OCI-0821527. Calculations were also conducted at the LION clusters at the Pennsylvania State University and at the National Energy Research Scientific Computing Center, which is supported by the Office of Science of the US Department of Energy under Contract No. DE-AC02-05CH11231.

References

[1] Wang J, Neaton JB, Zheng H, Nagarajan V, Ogale SB, Liu B, et al. Science 2003;299:1719.
[2] Lu J, Gunther A, Schrettle F, Mayr F, Krohns S, Lunkenheimer P, et al. Eur Phys J B 2010;75:451.
[3] Catalan G, Scott JF. Adv Mater 2009;21:2463.
[4] Amirov AA, Batdalov AB, Kallaev SN, Omarov ZM, Verbenko IA, Razumovskaya ON, et al. Phys Solid State 2009;51:1189.
[5] Lebeugle D, Colson D, Forget A, Viret M, Bataille AM, Gukasov A. Phys Rev Lett 2008;100:227602.
[6] Tutuncu HM, Srivastava GP. J Appl Phys 2008;103:083712.
[7] Rovillain P, Cazayous M, Gallais Y, Sacuto A, Lobo R, Lebeugle D, et al. Phys Rev B 2009;79:180411.
[8] Lobo RPSM, Moreira RL, Lebeugle D, Colson D. Phys Rev B 2007;76:172105.
[9] Haumont R, Kreisel J, Bouvier P, Hippert F. Phys Rev B 2006;73:132101.
[10] Goffinet M, Hermet P, Bilc DI, Ghosez P. Phys Rev B 2009;79:014403.
[11] Fukumura H, Matsui S, Harima H, Takahashi T, Itoh T, Kisoda K, et al. J Phys Condens Matter 2007;19:365224.
[12] Neaton JB, Ederer C, Waghmare UV, Spaldin NA, Rabe KM. Phys Rev B 2005;71:014113.
[13] Kubel F, Schmid H. Acta Crystallogr Sect B Struct Sci 1990;46:698.
[14] Lebeugle D, Colson D, Forget A, Viret M, Bonville P, Marucco JF, et al. Phys Rev B 2007;76:024116.
[15] Phapale S, Mishra R, Das D. J Nucl Mater 2008;373:137.
[16] Anisimov VI, Zaanen J, Andersen OK. Phys Rev B 1991;44:943.
[17] Chen JR, Wang WL, Li JB, Rao GH. J Alloys Compd 2008;459:66.
[18] Soffge F, von Horsten W. J Magn Magn Mater 1986;59:135.
[19] Singh MK, Prellier W, Singh MP, Katiyar RS, Scott JF. Phys Rev B 2008;77:144403.
[20] Redfern SAT, Wang C, Hong JW, Catalan G, Scott JF. J Phys Condens Matter 2008;20:452205.
[21] Nakamura S, Soeya S, Ikeda N, Tanaka M. J Appl Phys 1993;74:5652.
[22] Cazayous M, Gallais Y, Sacuto A, de Sousa R, Lebeugle D, Colson D. Phys Rev Lett 2008;101:037601.
[23] Singh MK, Katiyar RS, Scott JF. J Phys Condens Matter 2008;20:252203.
[24] Kittel C. Introduction to solid state physics. Hoboken (NJ): Wiley; 2005.
[25] Burns G. Solid State Commun 1980;35:811.
[26] Ho JC, Dandekar DP. Phys Rev B 1984;30:2117.
[27] Ahrens M, Merkle R, Rahmati B, Maier J. Physica B 2007;393:239.
[28] Cardona M, Kremer RK, Lauck R, Siegle G, Serrano J, Romero AH. Phys Rev B 2007;76:075211.
[29] Duran A, Morales F, Fuentes L, Siqueiros JM. J Phys Condens Matter 2008;20:085219.
[30] Romero AH, Cardona M, Kremer RK, Lauck R, Siegle G, Serrano J, et al. Phys Rev B 2008;78:224302.
[31] Cardona M, Kremer RK, Lauck R, Siegle G, Munoz A, Romero AH. Phys Rev B 2009;80:195204.
[32] Kilian O, Allan G, Wirtz L. Phys Rev B 2009;80:245208.
[33] Shaltaf R, Gonze X, Cardona M, Kremer RK, Siegle G. Phys Rev B 2009;79:075204.
[34] Hermet P, Goffinet M, Ghosez P. J Appl Phys 2009;105:036108.
[35] Hermet P, Goffinet M, Kreisel J, Ghosez P. Phys Rev B 2007;75:220102.
[36] Tutuncu HM, Srivastava GP. Phys Rev B 2008;78:235209.
[37] Tutuncu HM, Srivastava GP. J Appl Phys 2009;105:036108; . J Appl Phys 2009;105:036109.
[38] Zinenko VI, Pavlovskii MS. JETP Lett 2008;87:288.
[39] Cochran W, Cowley RA. J Phys Chem Solids 1962;23:447.
[40] Wang Y, Wang JJ, Wang WY, Mei ZG, Shang SL, Chen LQ, et al. J Phys Condens Matter 2010;22:202201.
[41] Wang Y, Saal JE, Wang JJ, Saengdeejing A, Shang SL, Chen LQ, et al. Phys Rev B 2010;82:081104.
[42] Dudarev SL, Peng LM, Savrasov SY, Zuo JM. Phys Rev B 2000;61:2506.
[43] Baroni S, de Gironcoli S, Dal Corso A, Giannozzi P. Rev Mod Phys 2001;73:515.
[44] Wallace DC. Thermodynamics of crystals. New York: John Wiley & Sons; 1972.
[45] Blöchl PE. Phys Rev B 1994;50:17953.
[46] Kresse G, Joubert D. Phys Rev B 1999;59:1758.
[47] Kornev IA, Lisenkov S, Haumont R, Dkhil B, Bellaiche L. Phys Rev Lett 2007;99:227602.
[48] Luo XH, Zhou W, Ushakov SV, Navrotsky A, Demkov AA. Phys Rev B 2009;80:134119.
[49] Savrasov SY, Kotliar G. Phys Rev Lett 2003;90:056401.
[50] Shang SL, Sheng G, Wang Y, Chen LQ, Liu ZK. Phys Rev B 2009;80:052102.
[51] Perdew JP, Chevary JA, Vosko SH, Jackson KA, Pederson MR, Singh DJ, et al. Phys Rev B 1992;46:6671.
[52] Sosnowska I, Schaffer W, Kockelmann W, Andersen KH, Troyanchuk IO. Appl Phys A Mater Sci Process 2002;74:S1040.
[53] Gao F, Yuan Y, Wang KF, Chen XY, Chen F, Liu JM. Appl Phys Lett 2006;89:102506.
[54] Ihlefeld JF, Podraza NJ, Liu ZK, Rai RC, Xu X, Heeg T, et al. Appl Phys Lett 2008;92:142908.
[55] Gajdos M, Hummer K, Kresse G, Furthmuller J, Bechstedt F. Phys Rev B 2006;73:045112.
[56] Ravindran P, Vidya R, Kjekshus A, Fjellvag H, Eriksson O. Phys Rev B 2006;74:224412.
[57] Ju S, Cai TY, Guo GY. J Chem Phys 2009;130:214708.
[58] Kamba S, Nuzhnyy D, Savinov M, Sebek J, Petzelt J, Prokleska J, et al. Phys Rev B 2007;75:024403.
[59] Zbiri M, Schober H, Johnson MR, Rols S, Mittal R, Su YX, et al. Phys Rev B 2009;79:064511.
[60] Sears VF. Neutron News 1992;3:26.
[61] Drulis M, Konieczny K. Mater Sci Eng B Solid State Mater Adv Technol 2000;72:19.